Benchmarking density-functional-theory calculations of rotational *g* tensors and magnetizabilities using accurate coupled-cluster calculations

Ola B. Lutnæs,[1,a] Andrew M. Teale,[1] Trygve Helgaker,[1] David J. Tozer,[2] Kenneth Ruud,[3] and Jürgen Gauss[4]

[1]*Department of Chemistry, Centre for Theoretical and Computational Chemistry, University of Oslo, P.O.B. 1033 Blindern, Oslo N-0315, Norway*
[2]*Department of Chemistry, Durham University, South Road, Durham DH1 3LE, United Kingdom*
[3]*Department of Chemistry, Centre for Theoretical and Computational Chemistry, University of Tromsø, Tromsø N-9037, Norway*
[4]*Institut für Physikalische Chemie, Universität Mainz, Mainz D-55099, Germany*

An accurate set of benchmark rotational *g* tensors and magnetizabilities are calculated using coupled-cluster singles-doubles (CCSD) theory and coupled-cluster single-doubles-perturbative-triples [CCSD(T)] theory, in a variety of basis sets consisting of (rotational) London atomic orbitals. The accuracy of the results obtained is established for the rotational *g* tensors by careful comparison with experimental data, taking into account zero-point vibrational corrections. After an analysis of the basis sets employed, extrapolation techniques are used to provide estimates of the basis-set-limit quantities, thereby establishing an accurate benchmark data set. The utility of the data set is demonstrated by examining a wide variety of density functionals for the calculation of these properties. None of the density-functional methods are competitive with the CCSD or CCSD(T) methods. The need for a careful consideration of vibrational effects is clearly illustrated. Finally, the pure coupled-cluster results are compared with the results of density-functional calculations constrained to give the same electronic density. The importance of current dependence in exchange–correlation functionals is discussed in light of this comparison. © *2009 American Institute of Physics*. [doi:10.1063/1.3242081]

I. INTRODUCTION

In recent decades, density-functional theory (DFT)[1,2] has become the most frequently applied methodology in quantum-chemical applications. This success has been a result of an attractive balance between the accuracy of the results obtained and low computational cost. The Achilles' heel of the method, however, is the need to approximate the unknown exchange-correlation (XC) functional, $E_{xc}[\rho]$. The lack of a systematic hierarchy of DFT functionals that converge to the exact $E_{xc}[\rho]$ means that, to assess the accuracy of the plethora of XC functionals in common use, benchmarking against accurate experimental or theoretical data is essential. The focus of this paper is the generation of and comparison with the latter.

Typically, the development of new DFT functionals has emphasized the importance of thermochemical properties, which play such a central role in chemistry. Nowadays, however, DFT is often also used to study response properties, representing the interaction of molecular systems with externally applied electromagnetic fields. Their calculation provides different challenges for $E_{xc}[\rho]$ approximations. In the present paper, we consider two related second-order magnetic response properties, namely, rotational *g* tensors and magnetizabilities.

In contrast with DFT, the coupled-cluster methodology provides a systematic route toward the exact description of the electronic system.[3] Thus, while the full configuration-interaction (FCI) wave function is computationally inaccessible for all but the smallest systems, the coupled-cluster method provides a robust framework for the calculation of molecular properties within a well-defined hierarchy of increasingly accurate methods. Truncating the coupled-cluster expansion at the level of double excitations, we obtain the coupled-cluster singles-doubles (CCSD) model of reasonable but usually not high accuracy. For higher accuracy, triple excitations are included in a perturbative manner at the coupled-cluster singe-doubles-perturbative-triples [CCSD(T)] level of theory. The latter has been shown to give high-accuracy results in a variety of applications and is typically the benchmark against which other methodologies are compared.

Recently, it has become possible to utilize DFT and coupled-cluster methods in conjunction with (rotational) London atomic orbitals (LAOs)[4–7] to calculate a variety of magnetic properties. In the present paper, we focus on a set of 28 small molecules in order to provide a set of accurate benchmark data. Basis-set extrapolation techniques are employed to obtain estimates of the basis-set-limit quantities. These results provide a useful data set for benchmarking less accurate *ab initio* methods since one can compare results within the Born–Oppenheimer approximation on an equal footing. By contrast, in comparisons with experimental data, a number of other effects plays an important role, notably,

---

a)Electronic mail: o.b.lutnas@kjemi.uio.no.

the effects of molecular vibrations, rotations and interactions with the surroundings. Since rotational g tensors can be determined experimentally with a very high accuracy,[8–10] we account for these effects when comparing our benchmark quantities with experimental data. We refrain from performing a similar comparison for the magnetizabilites as the experimental results are less well characterized, with error bars that do not allow for a meaningful discrimination between *ab initio* methods.

In the literature, a number of assessments of DFT functionals in the calculation of magnetic response properties have been reported.[11–21] However, a consistent set of *ab initio* data for comparison has been lacking (although for nuclear shielding constants some large sets of benchmark data have been reported[22,23]). In the present work, we address this shortcoming by providing such a set of rotational g tensors and magnetizabilities, calculated using LAOs at the CCSD and CCSD(T) levels of theory. A similar set of nuclear shielding and spin-rotation constants will be reported in a forthcoming publication.

In Sec. II, we briefly review the calculation of magnetic properties with LAOs in DFT and coupled-cluster methodologies, along with the technique we employ to calculate the zero-point vibrational corrections (ZPVCs) that are essential for a comparison with experiment. The use of optimized-effective potentials (OEPs)[24,25] and constrained-search[26] methods for the calculation of magnetic properties is also outlined. In Sec. III, we give some computational details of our calculations, including the basis-set extrapolation techniques used to estimate the basis-set-limit quantities. In Sec. IV, a summary of our results is presented (extensive extra information may be found in the supplementary material[27]). The benchmark data set is presented in Sec. IV A and errors relative to experimental data, with and without vibrational corrections, are discussed, along with details of convergence with respect to basis set and coupled-cluster excitation level. In Sec. IV B, we use the accurate benchmark data set to investigate the performance of a variety of XC functionals, paying particular attention to the use of OEP methods for the orbital-dependent forms. In Sec. IV C, we compare the performance of coupled-cluster methods with DFT calculations constrained to reproduce the same coupled-cluster density. Finally, in Sec. V, we give some concluding remarks.

II. THEORY

The rotational g tensor, $\mathbf{g}$, and magnetizability tensor, $\boldsymbol{\xi}$, are examples of second-order magnetic properties and can be identified as the derivatives

$$\mathbf{g} = -\frac{1}{\mu_N}\left.\frac{d^2 E}{d\mathbf{B}d\mathbf{J}}\right|_{\mathbf{B},\mathbf{J}=0}, \tag{1}$$

$$\boldsymbol{\xi} = -\left.\frac{d^2 E}{d\mathbf{B}^2}\right|_{\mathbf{B}=0}, \tag{2}$$

where E is the energy, $\mathbf{B}$ is the external magnetic field, μ_N is the nuclear magneton, and $\mathbf{J}$ is the rotational angular momentum. In these equations, and throughout this paper, atomic units are used unless otherwise indicated.

A. Ensuring gauge-origin independence

A difficulty in the calculation of accurate molecular magnetic properties stems from the fact that, in general, the use of approximate wave functions leads to an unphysical dependence on the gauge origin of the magnetic vector potential. To circumvent this problem in the present work, we use LAOs, also known as gauge-including atomic orbitals.[28] London first proposed imposing gauge-origin independence in molecular calculations by attaching field-dependent complex phase factors to the atomic orbitals.[29] The use of these orbitals for the calculation of magnetic properties is now widespread and often preferred to other procedures for imposing gauge-origin independence due to the more rapid convergence of the properties obtained with respect to the size of basis set employed. Generalized to rotating molecules,[6] the rotational LAOs are defined as

$$\omega_\mu(\mathbf{B},\mathbf{J}) = \exp\left[-i\left(\tfrac{1}{2}\mathbf{B} \times (\mathbf{R}_\mu - \mathbf{R}_O) - \mathbf{I}^{-1}\mathbf{J} \times \mathbf{R}_\mu\right) \cdot \mathbf{r}\right]\chi_\mu \tag{3}$$

where χ_μ is a usual atomic basis function, $\mathbf{R}_O$ is the origin of the vector potential, and $\mathbf{I}^{-1}$ is the inverse of the moment-of-inertia tensor. Use of the rotational LAOs Eq. (3) ensures gauge-origin independence and rapid basis-set convergence of rotational g tensors as well as magnetizabilities, which are then (with the center of mass $\mathbf{R}_{CM}$ as the gauge origin for the magnetizability) related as[6]

$$\mathbf{g} = -4m_p(\boldsymbol{\xi}^{LAO} - \boldsymbol{\xi}_{CM}^{dia})\mathbf{I}_{nuc}^{-1}$$
$$+ \frac{1}{2\mu_N}\sum_K Z_K(\mathbf{R}_K^T\mathbf{R}_K\mathbf{I}_3 - \mathbf{R}_K\mathbf{R}_K^T)\mathbf{I}_{nuc}^{-1}, \tag{4}$$

where m_p is the proton mass, $\boldsymbol{\xi}^{LAO}$ is the magnetizability tensor calculated with London orbitals, $\boldsymbol{\xi}_{CM}^{dia}$ is the diamagnetic contribution to the magnetizability tensor calculated with conventional orbitals and the gauge origin at the center of mass, and the sum is over all nuclei with charges Z_K and positions $\mathbf{R}_K$. This relationship means that the implementation of rotational g tensors can be achieved as a straightforward extension to any implementation of LAO magnetizabilities. We use the implementation of LAOs in the DALTON quantum-chemistry package for the Hartree–Fock and Kohn–Sham calculations,[4–6] and the recent implementation in the Mainz–Austin–Budapest version of the ACES II package for the coupled-cluster calculations.[6,7]

B. Comparison with experimental values

Experimentally, the magnetizability is often poorly determined or only known in the liquid or solid state, making comparisons between calculated and experimental results difficult. In contrast, gas-phase rotational g tensors are known with very high accuracy. When a molecule rotates, it acquires a magnetic moment proportional to its angular momentum. In an external magnetic field, the Zeeman interaction between this magnetic moment and the external magnetic induction causes a shift in the rotational energy levels. This shift can be observed in gas-phase molecular-beam[8] and microwave Zeeman[9,10] experiments and may be expressed as

$$\Delta E = -\mu_N \mathbf{B}^T \mathbf{g} \mathbf{J}, \tag{5}$$

where $\mathbf{g}$ is the dimensionless 3×3 rotational g tensor. Furthermore, since the rotational g tensor is determined experimentally from specific rotational-state transitions where the angular-momentum quantum number usually does not exceed $J=5$ (sometimes even the transition $J=0 \rightarrow 1$ is used, see the references of experimental measurements in Table II), we expect the effect of centrifugal distortion of the molecule on the measured g tensor to be small.

The high accuracy with which rotational g tensors can be determined experimentally makes them excellent candidates for testing the accuracy of *ab initio* electronic structure methods provided vibrational effects are taken into account. A variety of methods has been used to calculate these quantities previously, including Hartree–Fock theory,[6,30–32] multiconfigurational self-consistent-field (MCSCF) theory,[33–40] Møller–Plesset theory,[39,41,42] coupled-cluster theory,[39,41] the second-order polarization-propagator approximation (SOPPA),[39,43–45] the CCSD polarization-propagator approximation (CCSDPPA),[46–49] the SOPPA using CCSD amplitudes [SOPPA(CCSD)],[39,50] FCI theory[51–53] and DFT.[5,11,54] In the present work, we calculate the ZPVCs to the rotational g tensor and the magnetizability using perturbation theory, following Ref. 40 using DFT.

C. Optimized-effective potential and constrained-search calculations

In addition to using standard DFT implementations for calculating magnetizabilities and rotational g tensors described in Refs. 4–6, we employ OEP evaluations of the orbital-dependent DFT functionals we consider.[24,25] Specifically, we employ the Yang–Wu OEP scheme,[55,56] in which the Kohn–Sham effective potential, $v_s(\mathbf{r})$, is expanded as

$$v_s(\mathbf{r}) = v_{\text{ext}}(\mathbf{r}) + v_0(\mathbf{r}) + \sum_t b_t g_t(\mathbf{r}), \tag{6}$$

where $v_{\text{ext}}(\mathbf{r})$ is the external potential, $v_0(\mathbf{r})$ is a fixed reference potential, and the final term is an expansion in an auxiliary basis of Gaussian functions $g_t(\mathbf{r})$. The parameters b_t can then be determined by a direct minimization of the total electronic energy with respect to these parameters using an approximate Newton scheme.[56] For the reference potential, we use a slightly modified Fermi–Amaldi[57] potential

$$v_0(\mathbf{r}) = \left(1 - \frac{\eta}{N} \right) v_J^{\text{ref}}(\mathbf{r}), \tag{7}$$

where η is the proportion of Hartree–Fock-type exchange in the XC energy functional employed, N is the number of electrons, and $v_J^{\text{ref}}(\mathbf{r})$ is the Coulomb potential associated with a fixed reference density. This choice of reference potential ensures the appropriate asymptotic behavior of the XC potential for the functionals, containing an amount η of orbital-dependent exchange, considered in the present work. In the case of the Coulomb-attenuated functional CAM-B3LYP, the amount η is determined by the long-range exchange contribution. Once the OEP for a given functional is determined, the magnetic properties are calculated in the conventional uncoupled manner.

The constrained search provides an alternative way to determine multiplicative Kohn–Sham potentials. Rather than minimizing an approximate energy expression, the constrained search returns the Kohn–Sham potential, orbitals, and eigenvalues associated with a given density. In the present work, we utilize the constrained-search[26] scheme of Wu and Yang,[58] denoted as WY, to calculate the Kohn–Sham quantities associated with the CCSD and CCSD(T) densities. The scheme is computationally similar to that of the OEP method described above. For a given input density ρ_{in}, we perform an unconstrained maximization of the functional,

$$W_s[\Psi_{\text{det}}, v(\mathbf{r})] = 2 \sum_i^{N/2} \langle \varphi_i | -\tfrac{1}{2} \nabla^2 | \varphi_i \rangle$$

$$+ \int \{ v_{\text{ext}}(\mathbf{r}) + v_0(\mathbf{r}) \} \{ \rho(\mathbf{r}) - \rho_{\text{in}}(\mathbf{r}) \} d\mathbf{r}$$

$$+ \int \sum_t b_t g_t(\mathbf{r}) \{ \rho(\mathbf{r}) - \rho_{\text{in}}(\mathbf{r}) \} d\mathbf{r}, \tag{8}$$

with respect to the parameters b_t, where the orbitals are the solutions to Kohn–Sham equations with the potential of Eq. (6). The maximization is carried out using a quasi-Newton algorithm as described in Ref. 58. The WY scheme is utilized in the present work to calculate rotational g tensors and magnetizabilities. For molecules in a magnetic field, the XC energy depends not only on the density $\rho(\mathbf{r})$ but also on the current density $\mathbf{j}(\mathbf{r})$. The dependence on the latter is usually neglected. The calculation of WY quantities based on CCSD and CCSD(T) densities in comparison with the pure CCSD and CCSD(T) values can therefore give an indication of the importance of the current density in determining these magnetic properties.

III. COMPUTATIONAL DETAILS

A set of 28 molecules (see the first column of Table II) was chosen to provide a challenging and varied benchmark set amenable to coupled-cluster calculations with large basis sets. Molecular geometries optimized at the CCSD(T)/cc-pVTZ level were used throughout; the geometries are given in the supplementary material.[27] As discussed in the previous section, LAOs were employed to ensure gauge-origin independence of the results obtained. A range of basis sets was employed from Dunning's correlation-consistent families:[59–62] cc-pVXZ, cc-pCVXZ, aug-cc-pVXZ and aug-cc-pCVXZ with $X=$D, T, and Q. Spherical-harmonic basis functions were utilized throughout. To establish a benchmark data set, calculations were carried out using Hartree–Fock, CCSD[63] and CCSD(T)[64] wave functions with each basis set. In the coupled-cluster calculations, all electrons were correlated.

To provide an estimate of the Hartree–Fock basis-set-limit properties $P_{\text{HF},\infty}$, we used the extrapolation[65]

$$P_{\text{HF},\infty} = \frac{P_{\text{HF},X} \exp(\alpha X) - P_{\text{HF},Y} \exp(\alpha Y)}{\exp(\alpha X) - \exp(\alpha X)}, \tag{9}$$

with $\alpha=1.63$, and where X and Y are the cardinal numbers of the two basis sets used in the extrapolation, and $P_{\text{HF},X}$ is the

property calculated at the Hartree–Fock level with basis X.[65] To provide an estimate of the properties from the correlated wave-function methods in the limit of a complete basis set, we used the expression

$$P_\infty = P_{\text{HF},\infty} + \frac{X^3 P_{\text{corr},X} - Y^3 P_{\text{corr},Y}}{X^3 - Y^3}, \tag{10}$$

where P_∞ is the extrapolated value of the property and $P_{\text{corr},X}$ is the correlation contribution to the property calculated with cardinal number X.[66]

In the DFT calculations, a variety of XC functionals was employed in several categories: The local density approximation (LDA),[67,68] the generalized gradient approximations (GGAs) BLYP,[69,70] PBE,[71] and KT2[72] (the latter developed specifically with magnetic properties in mind), the hybrid functionals B3LYP,[73,74] B97–2,[75] B97–3,[76] and PBE0,[77] and the range-separated hybrid functional CAM-B3LYP.[78] To adhere strictly to the Kohn–Sham framework, the OEP method was also applied for the latter two categories, the results being denoted as O-B3LYP, O-B97-2, O-B97-3, O-PBE0, and O-CAMB3LYP. A number of previous studies considered the calculation of magnetic properties using multiplicative Kohn–Sham potentials, demonstrating consistent improvements.[11–21]

To examine the connection between the coupled-cluster and DFT methodologies further, the properties were also calculated from Kohn–Sham effective potentials determined to give the coupled-cluster densities via the WY constrained-search method, denoted WY(CCSD) and WY[CCSD(T)]. In the OEP/WY calculations, the auxiliary basis set used in the expansion in Eq. (6) was chosen to be the same as the primary orbital basis set. To give an indication whether this choice was sufficient, we also applied the method to the LDA and GGA functionals, for which the same results should be obtained as in the conventional evaluations; in these calculations, we obtained mean and mean absolute relative deviations agreeing to better than 0.1% in the largest basis set considered. The OEP and WY procedures were both carried out with a second-order optimization scheme.[56,58] The convergence tolerance on the largest absolute value of the gradient elements and the filter used in the singular-value decomposition were set to 10^{-6}. All coupled-cluster property calculations were performed using the Mainz–Austin–Budapest version of the ACES II program.[79] The remaining calculations were performed using a development version of DALTON.[80]

IV. RESULTS

A. The benchmark data set

1. Rotational g tensors

We commence by examining the basis-set convergence of the Hartree–Fock and coupled-cluster g tensors. For the four basis-set families, cc-pVXZ, cc-pCVXZ, aug-cc-pVXZ, and aug-cc-pCVXZ, the mean errors (MEs), mean absolute errors (MAEs), maximum absolute errors (MaxEs), mean relative errors (MREs), mean absolute relative errors (MAREs), and standard deviations (SDs) relative to the vibrationally corrected experimental data are presented in

Table I. The vibrational corrections were calculated at the B3LYP/aug-cc-pCVTZ level using the method of Ref. 40 and subtracted from the experimental values to give a set of empirical equilibrium values, see Table II. The vibrational corrections obtained agree very well with the available MC-SCF values in Ref. 38. For the aug-cc-pCVQZ basis set, individual results are presented in Table II. For the smaller basis sets, individual results are provided as part of the supplementary material.[27]

In Table I, the errors in rotational g tensors relative to the empirical equilibrium values are presented, excluding the multireference O_3 molecule from the analysis; for the full analysis and individual g-tensor elements, see the supplementary material.[27] An inspection of the table shows that the addition of core-correlating functions to either the standard or augmented basis-set families leads to only modest changes in the results; the addition of diffuse functions is much more important. It is also noteworthy that, beyond $X = 3$, the Hartree–Fock results are quite stable for all basis sets, reflecting their rapid exponential convergence toward the basis-set limit as demonstrated by Eq. (9). For the coupled-cluster results, convergence is slower because of the difficulties associated with describing the electronic cusp, see Eq. (10).

It is gratifying to note that, in Table I, the smallest errors with respect to the empirical equilibrium constants are observed with the most advanced electronic-structure model in the largest one-electron basis set, namely, at the all-electron CCSD(T)/aug-cc-pCVQZ level of theory. We therefore choose to construct our benchmark data set by applying the extrapolation formulas in Eqs. (9) and (10) to the aug-cc-pCVTZ and aug-cc-pCVQZ results obtained with the CCSD(T) method, yielding the all-electron CCSD(T)/aug-cc-pCV[TQ]Z results.

In Table II, we present explicitly the results for the largest basis set employed for the Hartree–Fock, CCSD and CCSD(T) models, along with the CCSD(T)/aug-cc-pCV[TQ]Z benchmark data set, empirical equilibrium values, and experimental values. The errors with respect to both the empirical and experimental values and the benchmark data are presented in Table III. In each case, O_3 has been excluded from the error analysis; the full error analysis is reported in the supplementary material.[27] The results follow the trends expected, with the CCSD(T)/aug-cc-pCVQZ results being closest to the benchmark data set, from which it differs only by the application of basis-set extrapolation in the latter set. In both cases, the effect of adding vibrational corrections is striking, leading to a factor of 2 improvement in the errors, for example, the MARE of the benchmark set is reduced from 5.1% to 2.5%.

2. Magnetizabilities

As discussed in Sec. II, the calculation of rotational g tensors is closely related to that of magnetizabilities via Eq. (4). Given this close relationship, we expect that methods well suited to the calculation of rotational g tensors should also be well suited to the calculation of magnetizabilities. However, as discussed in Sec. II B, it is often difficult to

TABLE I. Rotational *g* tensors: Statistical errors for the molecules in Table II (excluding O_3) relative to empirical equilibrium results. Presented are MEs, MAEs, MaxEs, MREs (%), MAREs (%), and SDs.

Method	Basis	X	ME	MAE	MaxE	MRE	MARE	SD
RHF	cc-pVXZ	2	0.0035	0.0225	0.1876	−6.9	14.5	0.0393
		3	0.0050	0.0177	0.1756	−5.1	11.0	0.0356
		4	0.0043	0.0174	0.1877	−4.1	10.2	0.0362
	cc-pCVXZ	2	0.0035	0.0221	0.1772	−7.1	14.4	0.0382
		3	0.0045	0.0177	0.1762	−5.4	11.1	0.0349
		4	0.0039	0.0174	0.1884	−4.4	10.3	0.0362
	aug-cc-pVXZ	2	0.0063	0.0184	0.1745	−2.5	10.5	0.0385
		3	0.0045	0.0170	0.1911	−3.1	9.6	0.0367
		4	0.0040	0.0170	0.1914	−3.4	9.6	0.0365
	aug-cc-pCVXZ	2	0.0062	0.0182	0.1748	−2.7	10.5	0.0377
		3	0.0040	0.0169	0.1920	−3.6	9.7	0.0363
		4	0.0036	0.0170	0.1920	−3.7	9.7	0.0365
CCSD	cc-pVXZ	2	0.0004	0.0192	0.1035	−8.0	10.7	0.0303
		3	0.0039	0.0117	0.1063	−4.8	6.8	0.0200
		4	0.0031	0.0085	0.0975	−2.6	4.8	0.0169
	cc-pCVXZ	2	0.0004	0.0190	0.1009	−8.0	10.6	0.0298
		3	0.0020	0.0102	0.0892	−4.1	5.7	0.0177
		4	0.0032	0.0079	0.0943	−2.7	4.6	0.0164
	aug-cc-pVXZ	2	0.0062	0.0115	0.1045	−0.8	5.2	0.0213
		3	0.0028	0.0083	0.0967	−1.7	4.0	0.0170
		4	0.0035	0.0074	0.0973	−1.6	4.0	0.0162
	aug-cc-pCVXZ	2	0.0051	0.0104	0.1045	−1.3	4.5	0.0201
		3	0.0026	0.0067	0.0877	−1.4	3.6	0.0151
		4	0.0032	0.0065	0.0926	−1.5	3.9	0.0155
CCSD(T)	cc-pVXZ	2	−0.0019	0.0181	0.1037	−7.4	9.9	0.0286
		3	0.0015	0.0096	0.0492	−3.8	5.6	0.0145
		4	0.0007	0.0062	0.0351	−1.4	3.3	0.0101
	cc-pCVXZ	2	−0.0019	0.0179	0.1016	−7.4	9.8	0.0281
		3	−0.0004	0.0081	0.0376	−3.0	4.5	0.0126
		4	0.0007	0.0057	0.0318	−1.4	3.1	0.0095
	aug-cc-pVXZ	2	0.0041	0.0103	0.0575	0.2	4.9	0.0174
		3	0.0005	0.0064	0.0347	−0.4	3.3	0.0108
		4	0.0012	0.0049	0.0329	−0.2	2.5	0.0091
	aug-cc-pCVXZ	2	0.0030	0.0092	0.0574	−0.3	4.3	0.0159
		3	0.0003	0.0046	0.0276	0.0	2.4	0.0084
		4	0.0007	0.0044	0.0294	0.0	2.4	0.0084

obtain reliable gas-phase experimental data for comparison with calculated results. As such, we refrain from comparing our results directly with experimental data.

In Table IV, we present magnetizabilities calculated at the Hartree–Fock, CCSD and CCSD(T) levels of theory in the aug-cc-pCVQZ basis set as well as the CCSD(T)/aug-cc-pCV[TQ]Z benchmark results. Vibrational corrections calculated at the B3LYP/aug-cc-pCVTZ level of theory are presented in the final column. In the absence of reliable experimental data, the errors in Table V are quoted relative to the benchmark data set only. Values for all other basis sets considered may be found in the supplementary material.[27] The utility of this data set for benchmarking purposes is demonstrated in the next section.

B. Benchmarking the DFT functionals

In the present section, we examine the accuracy that several popular XC functionals provide in the calculation of rotational *g* tensors and magnetizabilities, by comparison with the all-electron CCSD(T)/aug-cc-pCV[TQ]Z bench-

mark data and, in the case of rotational *g* tensors, with experimental data. For all the orbital-dependent XC functionals, we also examine the corresponding OEP results.

1. Rotational *g* tensors

The errors for the conventional DFT/aug-cc-pCVQZ results relative to the benchmark set, empirical equilibrium values, and experimental values are contained in Table VI. In evaluating the statistical errors, the O_3 results were excluded from the analysis; the full analysis is presented in the supplementary material.[27] The *g* tensors for all the individual molecules are given in the supplementary material.[27]

From an inspection of Table VI, a number of trends becomes apparent. First, we consider the comparison with experimental values. Here the LDA functional stands out as being particularly poor with MARE and MRE values of 10.4% and −7.8% respectively, the SD is also rather large. For the GGA functionals BLYP and PBE, the MRE and SD values are improved but the MARE values remain similar. The KT2 functional, which was designed specifically for the

TABLE II. Rotational *g* tensors: Coupled-cluster and experimental values.

Molecule	RHF[a]	CCSD[b]	CCSD(T)[b]	CCSD(T)[c]	Emp. eq.[d]	Exp.
HF	0.7627	0.7535	0.7527	0.7542	0.7543	0.7416[e]
CO	−0.2816	−0.2669	−0.2678	−0.2681	−0.2676	−0.2689[f]
$^{15}N_2$	−0.2699	−0.2576	−0.2591	−0.2591	−0.2577	−0.2593[g]
H_2O	0.6834	0.6725	0.6707	0.6717	0.686	0.657[h]
	0.7323	0.7281	0.7284	0.7303	0.733	0.718[h]
	0.6641	0.6550	0.6547	0.6563	0.654	0.645[h]
$HC^{15}N$	−0.0773	−0.0846	−0.0882	−0.0882	−0.0872	−0.0904[i]
HOF	0.7011	0.6863	0.6840	0.6853	0.672	0.642[j]
	−0.0951	−0.1062	−0.1110	−0.1107	−0.108	−0.119[j]
	−0.0440	−0.0561	−0.0601	−0.0596	−0.060	−0.061[j]
O_3	−5.8380	−3.1399	−2.8833	−2.8980	−3.1333	−2.9877[k]
	−0.3915	−0.2470	−0.2243	−0.2247	−0.2360	−0.2295[k]
	−0.0669	−0.0725	−0.0744	−0.0741	−0.0777	−0.0760[k]
NH_3	0.5780	0.5755	0.5757	0.5770	0.5795	0.5654[l]
	0.5072	0.5084	0.5093	0.5107	0.5086	0.5024[l]
CH_2O (formaldehyde)	−2.7019	−2.8013	−2.8659	−2.8641	−2.8939	−2.9017[m]
	−0.2227	−0.2175	−0.2197	−0.2194	−0.2222	−0.2243[m]
	−0.0664	−0.0856	−0.0924	−0.0910	−0.0945	−0.0994[m]
CH_4	0.3033	0.3209	0.3231	0.3236	0.3217	0.3133[n]
C_2H_4	−0.3338	−0.3561	−0.3688	−0.3679	N/A	N/A
	−0.1143	−0.1110	−0.1123	−0.1118	N/A	N/A
	0.0612	0.0561	0.0538	0.0550	N/A	N/A
AlF	−0.0842	−0.0801	−0.0794	−0.0794	−0.0808	−0.0805[o]
CH_3F	0.2680	0.2731	0.2711	0.2724	0.277	0.265[p]
	−0.0550	−0.0586	−0.0606	−0.0601	−0.060	−0.062[p]
C_3H_4 (cyclopropene)	−0.0939	−0.0800	−0.0803	−0.0802	−0.0828	−0.0897[q]
	−0.1484	−0.1402	−0.1431	−0.1424	−0.1447	−0.1492[q]
	0.0627	0.0606	0.0592	0.0595	0.0586	0.0536[q]
FCCH	−0.0032	−0.0055	−0.0063	−0.0062	−0.0066	−0.0077[r]
$FC^{15}N$	−0.0479	−0.0483	−0.0487	−0.0487	−0.0499	−0.0504[s]
H_2S	0.3804	0.3945	0.3974	0.3978	0.378	0.355[t]
	0.1253	0.1778	0.1861	0.1883	0.216	0.195[t]
	0.1894	0.2234	0.2300	0.2321	0.208	0.209[t]
HCP	−0.0313	−0.0359	−0.0385	−0.0382	−0.0389	−0.0430[i]
HFCO	−0.4137	−0.4228	−0.4271	−0.4268	−0.4270	−0.4227[u]
	−0.0769	−0.0767	−0.0771	−0.0770	−0.0703	−0.0771[u]
	−0.0355	−0.0362	−0.0368	−0.0367	−0.0366	−0.0371[u]
H_2C_2O (ketene)	−0.4041	−0.4322	−0.4297	−0.4300	−0.4394	−0.4182[v]
	−0.0336	−0.0341	−0.0347	−0.0345	−0.0352	−0.0356[v]
	−0.0253	−0.0244	−0.0245	−0.0243	−0.0233	−0.0238[v]
LiF	0.0733	0.0691	0.0677	0.0678	0.0733	0.0737[w]
LiH	−0.6963	−0.6647	−0.6638	−0.6649	−0.6646	−0.6584[x]
N_2O	−0.0786	−0.0775	−0.0780	−0.0778	−0.0780	−0.0789[y]
OCS	−0.0285	−0.0277	−0.0280	−0.0279	−0.0282	−0.0288[z]
OF_2	−0.1429	−0.1846	−0.1977	−0.1972	−0.202	−0.213[aa]
	−0.0471	−0.0525	−0.0551	−0.0550	−0.057	−0.058[aa]
	−0.0610	−0.0642	−0.0672	−0.0671	−0.067	−0.068[aa]
H_4C_2O (oxirane)	−0.0807	−0.0876	−0.0910	−0.0905	−0.0905	−0.0946[bb]
	0.0360	0.0287	0.0259	0.0267	0.0256	0.0189[bb]
	0.0382	0.0371	0.0366	0.0369	0.0333	0.0318[bb]
PN	−0.2406	−0.2253	−0.2285	−0.2285	N/A	N/A
SO_2	−0.6766	−0.5927	−0.5985	−0.5988	−0.5929	−0.6043[cc]
	−0.1201	−0.1160	−0.1165	−0.1165	−0.1156	−0.1163[cc]
	−0.0882	−0.0868	−0.0869	−0.0873	−0.0888	−0.0887[cc]

[a]aug-cc-pCVQZ value.
[b]All-electron/aug-cc-pCVQZ value.
[c]All-electron/aug-cc-pCV[TQ]Z value.
[d]Empirical equilibrium value obtained by subtracting B3LYP/aug-cc-pCVTZ ZPVC from experimental value.
[e]Reference 92.
[f]Reference 93.
[g]Reference 94 sign from Ref. 95.
[h]Reference 96.
[i]Reference 97.
[j]Reference 98.
[k]Reference 99.
[l]Reference 100.
[m]Reference 9.
[n]Reference 101.

[o]Reference 102.
[p]Reference 103.
[q]Reference 104.
[r]Reference 105.
[s]Reference 106.
[t]Reference 107.
[u]Reference 108.
[v]Reference 109.
[w]Reference 110.
[x]Reference 111.
[y]Reference 112.
[z]Reference 113.
[aa]Reference 114.
[bb]Reference 115.
[cc]Reference 116.

TABLE III. Statistical errors in calculated rotational *g* tensors for the molecules Table II (excluding O_3).

Ref.	Err.	RHF[a]	CCSD[b]	CCSD(T)[b]	CCSD(T)[c]
CCSD(T)[c]	ME	0.0027	0.0022	−0.0005	0.0000
	MAE	0.0158	0.0036	0.0006	0.0000
	MaxE	0.1622	0.0628	0.0022	0.0000
	MRE	3.3	1.4	0.0	0.0
	MARE	9.0	2.1	0.5	0.0
	SD	0.0308	0.0094	0.0007	0.0000
Emp. eq.[d]	ME	0.0036	0.0032	0.0007	0.0012
	MAE	0.0170	0.0065	0.0044	0.0045
	MaxE	0.1920	0.0926	0.0294	0.0298
	MRE	3.7	1.5	0.0	0.0
	MARE	9.7	3.9	2.4	2.5
	SD	0.0365	0.0155	0.0084	0.0084
Exp.[e]	ME	0.0089	0.0086	0.0060	0.0065
	MAE	0.0194	0.0104	0.0076	0.0080
	MaxE	0.1998	0.1004	0.0424	0.0433
	MRE	3.0	1.2	−0.1	−0.1
	MARE	11.8	6.7	4.8	5.1
	SD	0.0370	0.0173	0.0108	0.0112

[a]aug-cc-pCVQZ basis.
[b]All-electron/aug-cc-pCVQZ basis.
[c]All-electron/aug-cc-pCV[TQ]Z basis.
[d]Empirical equilibrium values obtained by subtracting B3LYP/aug-cc-pCVTZ ZPVCs from experimental values.
[e]Experimental values in Table II.

calculation of magnetic properties, clearly stands out from the other functionals when compared with the experimental values; it has the lowest ME, MaxE, MRE, and SD values and is a substantial improvement over LDA and other GGA functionals. For the hybrid functionals B3LYP, B97-2, B97-3, and PBE0, the errors are also a considerable improvement over LDA and standard GGAs. However, although their MAE values are competitive with KT2, their ME, SD, and MaxE values are much worse. Finally, it is noteworthy that the CAM-B3LYP functional does not offer further improvement, the results being similar in quality to PBE0.

When performing comparisons directly with experiment, we neglect vibrational and rotational effects. Since rotational effects are small and most experimental measurements determine the *g* tensor from low rotational transitions, these are neglected in the present work. However, to correct for the much larger vibrational effects, we calculated ZPVCs at the B3LYP/aug-cc-pCVTZ level. These ZPVCs have then been subtracted from the experimental values in Table II to give the empirical equilibrium values listed in the same table. We now consider benchmarking the DFT functionals relative to this data.

It is noteworthy that, for all the DFT functionals in Table VI, the addition of vibrational corrections leads to a degradation in the quality of the results. While the conclusions above about the relative accuracy of the functionals based on the ME and SD values are still valid, these quantities consistently increase when ZPVCs are taken into account. Furthermore, the KT2 functional, which was outstanding when compared directly with experimental data, becomes comparable in quality to the B97-2 functional. The reduced quality of the KT2 functional in comparison with empirical values reflects the fact that the training data set used in its construction did

not properly take into account vibrational corrections. The data provided here suggest that some reparametrization may be desirable and highlight the need for a systematic benchmark data set as presented in the present work. Finally, comparing the DFT results with our CCSD(T) benchmark set, we observe a further systematic increase in the errors, although small. The modest size of this shift indicates that our CCSD(T) benchmark set is well converged toward the Born–Oppenheimer solutions.

We now turn our attention to the OEP results for rotational *g* tensors, the supplementary material[27] contains results for the individual molecules. As reported in our previous work,[11] the application of the OEP procedure to the calculation of *g* tensors leads to considerable improvements; see the statistical errors listed in Table VII. The O-B97-2 and O-B97-3 methods appear particularly impressive with all error measures improving over the KT2 functional. When ZPVCs are considered, a similar degradation in the quality of the results is observed, although the systematic improvement due to the application of the OEP procedure is maintained. Again a similar shift is observed on changing the comparison to the CCSD(T) benchmark data set. Among all the DFT methods presented, the best overall performance is given by the O-B97-3 method, which consistently has the lowest error measures compared with either experimental or empirical equilibrium values. In comparison with the CCSD(T) benchmark set, all the O-B97-3 measures except the MARE are the lowest among all XC functionals.

In Fig. 1, we present the normal distributions of the errors relative to our benchmark set for the DFT functionals considered here. The results are presented on a common scale to make them comparable with the CCSD results. Although the best DFT methods are a substantial improvement

TABLE IV. Magnetizabilities: Coupled-cluster values and B3LYP ZPVCs. All quantities are in SI units (10^{-30} J T^{-2}).

Molecule	RHF[a]	CCSD[b]	CCSD(T)[b]	CCSD(T)[c]	ZPVC[d]
HF	−172.7	−176.0	−176.7	−176.4	1.3
CO	−204.5	−210.1	−210.4	−209.5	18.5
N_2	−202.8	−206.0	−206.0	−205.2	36.0
H_2O	−231.3	−234.5	−235.5	−235.1	−0.7
HCN	−280.1	−273.8	−272.7	−271.8	1.3
HOF	−244.6	−238.6	−235.9	−235.4	3.6
O_3	580.5	164.8	118.6	121.5	25.5
NH_3	−287.4	−289.6	−290.8	−290.3	−2.1
CH_2O	−139.5	−132.1	−127.8	−127.4	3.3
CH_4	−313.7	−316.5	−317.5	−316.9	−3.3
C_2H_4	−354.7	−347.7	−346.1	−345.6	2.9
AlF	−399.4	−395.2	−396.2	−394.5	3.6
CH_3F	−318.0	−317.1	−316.3	−315.7	0.1
C_3H_4	−478.0	−481.5	−480.0	−478.9	5.8
FCCH	−452.2	−443.5	−442.7	−441.6	0.8
FCN	−378.0	−371.7	−370.9	−370.0	1.5
H_2S	−452.8	−454.7	−456.3	−455.1	−0.1
HCP	−511.5	−497.1	−494.4	−492.8	3.6
HFCO	−311.5	−309.0	−308.1	−307.2	1.7
H_2C_2O	−432.6	−425.6	−424.9	−423.9	−0.8
LiF	−190.9	−195.0	−196.0	−195.5	10.2
LiH	−125.3	−127.9	−127.9	−127.2	28.0
N_2O	−342.8	−340.8	−339.8	−339.1	2.3
OCS	−597.5	−587.9	−585.6	−584.1	2.1
OF_2	−271.6	−256.0	−247.8	−247.1	7.5
H_4C_2O	−544.8	−537.7	−536.0	−535.2	3.2
PN	−303.8	−312.5	−309.7	−308.2	58.1
SO_2	−301.8	−317.1	−316.7	−314.3	4.4

[a]aug-cc-pCVQZ values.
[b]All-electron/aug-cc-pCVQZ values.
[c]All-electron/aug-cc-pCV[TQ]Z values.
[d]B3LYP/aug-cc-pCVTZ.

over the LDA and standard GGA methods, they cannot compete with CCSD theory. However, all of the results presented in Fig. 1, including the CCSD results, are eclipsed by the very high quality of the CCSD(T) results. The quality of the CCSD(T) results is clear in Table III, for the largest basis set considered, where all the error measures relative to benchmark, empirical equilibrium, or experimental values are systematically and substantially improved over the CCSD results.

To rationalize many of the trends observed, we present in Fig. 2 a simple comparison of the MREs relative to the

TABLE V. Magnetizabilities: Statistical errors for the results in Table IV (excluding O_3) relative to the CCSD(T)/aug-cc-pCV[TQ]Z benchmark data set. All quantities in SI units (10^{-30} JT^{-2}).

	RHF[a]	CCSD[b]	CCSD(T)[b]
ME	−3.7	−1.9	−0.9
MAE	7.2	2.1	0.9
MaxE	24.5	8.9	2.4
MRE	−1.1	−0.7	−0.3
MARE	2.5	0.7	0.3
SD	8.4	2.1	0.5

[a]aug-cc-pCVQZ basis.
[b]All-electron/aug-cc-pCVQZ basis.

CCSD(T) benchmark data set obtained with the various wave-function and DFT methods employed here. Whereas the wave-function methods approach the benchmark values from above, the DFT methods approach from below. Figure 2 is essentially unchanged when MREs relative to empirical values are used. Since the vibrational corrections systematically shift the experimental values upward (see Table II), it is clear that adding vibrational corrections to experimental values improves the agreement with the wave-function methods and worsens the agreement with the DFT methods.

What is also clear from Fig. 2 is that the quality of the functionals can be rationalized by grouping them in terms of the information on which they are based. The LDA model, which uses only the local density, performs poorly; addition of the density gradient improves results for the GGA group. Next, the addition of a dependence on the occupied orbitals leads to further improvement for the hybrid functionals. The application of the OEP method to these functionals brings them back into the Kohn–Sham framework, resulting in further improvement due to their improved virtual eigenvalue spectrum.[15–18] It is again noteworthy that the range separation introduced for the CAM-B3LYP and O-CAM-B3LYP methods does not lead to significant improvements in their respective groups. Since the DFT XC functionals are not

TABLE VI. Rotational *g* tensors: Statistical errors for the DFT/aug-cc-pCVQZ results (excluding O_3) relative to the CCSD(T)/aug-cc-pCV[TQ]Z benchmark data set, empirical equilibrium values, and experimental values.

Ref.	Err.	LDA	BLYP	PBE	KT2	B3LYP	B97-2	B97-3	PBE0	CAM[a]
CCSD(T)[b]	ME	−0.0184	−0.0250	−0.0211	−0.0114	−0.0173	−0.0120	−0.0134	−0.0122	−0.0142
	MAE	0.0305	0.0272	0.0249	0.0169	0.0184	0.0143	0.0147	0.0149	0.0149
	MaxE	0.5967	0.3014	0.3706	0.0873	0.2239	0.1542	0.1923	0.2528	0.2582
	MRE	−9.0	−5.5	−6.3	−1.2	−3.7	−2.4	−2.6	−3.8	−3.8
	MARE	13.2	16.5	13.1	8.9	10.2	6.3	6.1	6.0	7.6
	SD	0.0884	0.0441	0.0546	0.0237	0.0328	0.0255	0.0293	0.0384	0.0368
Emp. eq.[c]	ME	−0.0150	−0.0227	−0.0183	−0.0090	−0.0152	−0.0099	−0.0114	−0.0099	−0.0123
	MAE	0.0297	0.0255	0.0244	0.0167	0.0168	0.0139	0.0140	0.0155	0.0145
	MaxE	0.5669	0.2716	0.3408	0.0768	0.1941	0.1245	0.1625	0.2230	0.2285
	MRE	−8.4	−5.2	−5.7	−1.0	−3.3	−1.9	−2.0	−3.2	−3.5
	MARE	12.5	15.6	12.7	8.8	9.4	6.2	5.9	6.2	7.1
	SD	0.0872	0.0417	0.0525	0.0232	0.0308	0.0243	0.0278	0.0368	0.0350
Exp.[d]	ME	−0.0096	−0.0173	−0.0130	−0.0037	−0.0099	−0.0045	−0.0060	−0.0045	−0.0070
	MAE	0.0302	0.0199	0.0199	0.0116	0.0124	0.0105	0.0114	0.0142	0.0127
	MaxE	0.5591	0.2638	0.3330	0.0706	0.1863	0.1166	0.1547	0.2152	0.2207
	MRE	−7.8	−4.0	−4.9	−0.3	−2.7	−1.6	−1.7	−3.0	−3.1
	MARE	10.4	12.0	9.2	5.6	5.9	4.3	4.6	5.1	5.0
	SD	0.0867	0.0396	0.0510	0.0184	0.0295	0.0224	0.0267	0.0359	0.0347

[a]CAM-B3LYP functional.
[b]All-electron CCSD(T)/aug-cc-pCV[TQ]Z theory.
[c]Empirical equilibrium values obtained by subtracting B3LYP/aug-cc-pCVTZ ZPVCs from experimental values.
[d]Experimental values in Table II.

systematically improvable, the quality of the groups can overlap. A case in point here is the KT2 functional, which stands out from the GGA group of functionals as being competitive with the hybrid and OEP methods. Figure 2 is essentially an illustration of the lower rungs of Perdew's "Jacob's ladder" of functionals. For further improvements, it is likely

that dependence on all orbitals needs to be considered and the OEP method will play a vital role in these Kohn–Sham calculations. Some examples of such functionals are already appearing in the literature.[81–88]

Throughout our analysis, we excluded the O_3 molecule due to its multireference nature. As may be expected, its

TABLE VII. Rotational *g* tensors: Statistical errors for the DFT-OEP/aug-cc-pCVQZ results (excluding O_3) relative to the CCSD(T)/aug-cc-pCV[TQ]Z benchmark data set, empirical equilibrium values, and experimental values.

Ref.	Err.	O-B3LYP	O-B97-2	O-B97-3	O-PBE0	O-CAM[a]
CCSD(T)[b]	ME	−0.0131	−0.0076	−0.0077	−0.0068	−0.0088
	MAE	0.0156	0.0111	0.0108	0.0110	0.0121
	MaxE	0.1058	0.0814	0.0791	0.1014	0.0857
	MRE	−2.2	−1.0	−0.6	−1.9	−2.1
	MARE	10.1	6.2	6.0	5.9	8.3
	SD	0.0212	0.0173	0.0172	0.0231	0.0209
Emp.eq.[c]	ME	−0.0107	−0.0050	−0.0051	−0.0040	−0.0062
	MAE	0.0138	0.0106	0.0094	0.0108	0.0106
	MaxE	0.0760	0.0908	0.0885	0.1108	0.0912
	MRE	−1.9	−0.5	−0.1	−1.4	−1.8
	MARE	9.4	6.0	5.5	5.7	7.7
	SD	0.0189	0.0177	0.0169	0.0212	0.0186
Exp.[d]	ME	−0.0053	0.0003	0.0002	0.0013	−0.0009
	MAE	0.0091	0.0070	0.0062	0.0085	0.0078
	MaxE	0.0682	0.0696	0.0672	0.0896	0.0700
	MRE	−1.2	−0.1	0.3	−1.1	−1.3
	MARE	5.9	3.2	2.9	3.3	4.5
	SD	0.0153	0.0138	0.0133	0.0185	0.0158

[a]O-CAM-B3LYP method.
[b]All-electron CCSD(T)/aug-pCV[TQ]Z theory.
[c]Empirical equilibrium values obtained by subtracting B3LYP/aug-cc-pCVTZ ZPVCs from experimental values.
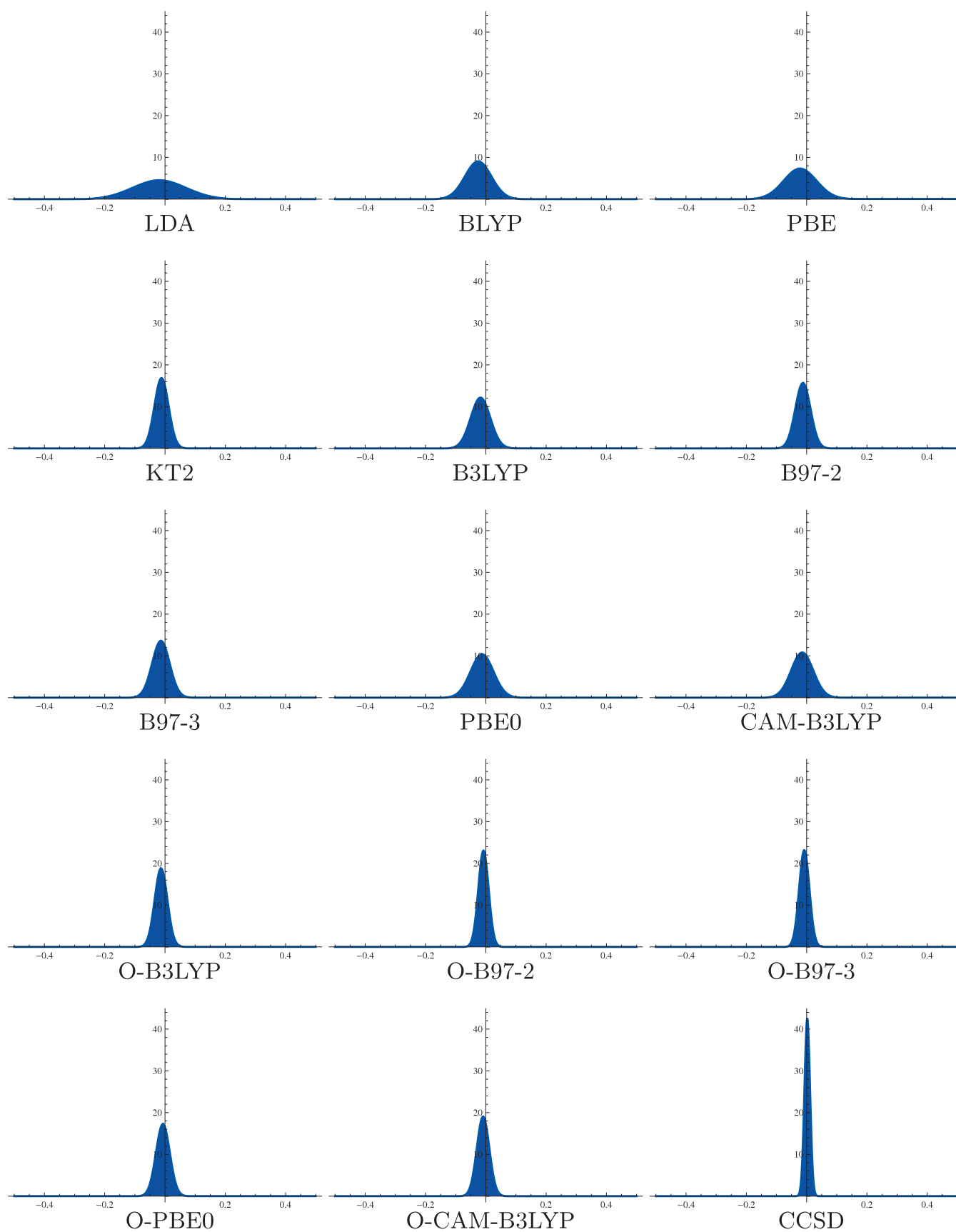[d]Experimental values in Table II.

FIG. 1. Normal distributions of the errors in the rotational *g* tensors relative to the CCSD(T)/aug-cc-pCV[TQ]Z benchmark data set for the set of molecules excluding O_3 using the aug-cc-pCVQZ basis set.
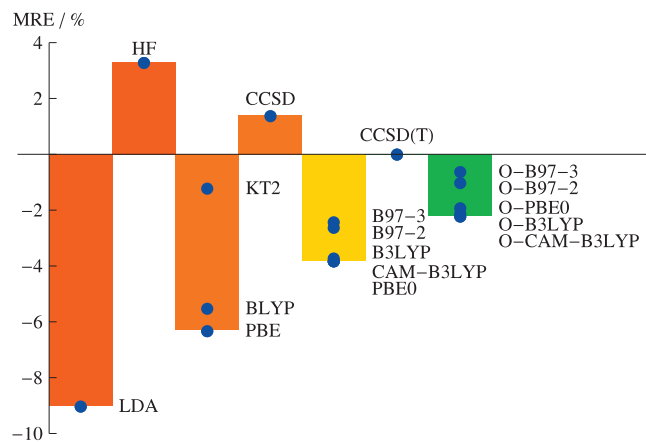
FIG. 2. MREs (%) in the calculation of rotational *g* tensors compared with the benchmark data set (excluding O_3) for the various wave function and DFT methods employed. The DFT results are grouped by functional type. The heights of the bars correspond to the largest MRE in each category.

inclusion leads to a significant degradation of the Hartree–Fock, CCSD, CCSD(T), and conventional hybrid DFT results. However, it is striking that the addition of O_3 has little effect on the errors for the LDA-, GGA-, and OEP-based Kohn–Sham functionals, all of which employ a local, multiplicative Kohn–Sham potential, see supplementary material for the details of the error analysis.[27] See Ref. [11] for further discussion of O_3.

2. Magnetizabilities

In the present section, we compare the DFT magnetizabilities with the data in Table IV, which contains magnetizabilities calculated with Hartree–Fock and coupled-cluster methods in the aug-cc-pCVQZ basis and the CCSD(T)/aug-cc-pCV[TQ]Z benchmark data set. The error measures of the conventional DFT results in the aug-cc-pCVQZ basis are presented in Table VIII. The calculated DFT magnetizabilities are given in the supplementary material[27] together with error measures for other basis sets.

The LDA, BLYP, and PBE results are consistently worse than the Hartree–Fock results on all the error measures, whereas the KT2 results are comparable with the Hartree–Fock results, with small improvements except in the ME and MRE measures. Similar statements hold for the B3LYP, B97-2, B97-3, and PBE0 hybrid functionals, the B3LYP results being superior. Remarkably, the only functional that consistently improves on the Hartree–Fock results is the CAM-B3LYP functional, which also represents approxi-

mately a factor of 2 improvement over the LDA functional but is still not competitive with the CCSD model.

In Table IX, the error measures of the OEP evaluated magnetizabilities for the orbital-dependent functionals, compared to the benchmark values of Table IV, are presented. For the O-B3LYP, O-B97-2, O-B973, and O-PBE0 methods, all error measures consistently improve on the conventional evaluations. For the O-CAM-B3LYP method, the ME, MAE, MRE, and MARE measures improve slightly, while the MaxE and SD measures degrade slightly. Normal distributions of errors relative to the CCSD(T) benchmark set are presented in Fig. 3. From this figure, it is clear that, while the ME is improved by the best DFT methods, the SD of the errors is not dramatically improved.

Given the close relationship between the magnetizabilities and *g* tensors shown in Eq. (4), it is interesting to compare the accuracies with which these properties are calculated. Comparing the MREs and MAREs in Tables VI and VII with those in Tables VIII and IX, the errors in the *g* tensor appear larger. However, noting from Eq. (4) that the first term is an electronic contribution that varies with the method employed, whereas the second term is a nuclear contribution constant for all methods, it is perhaps more instructive to consider the errors in the electronic contribution only. In practical calculations, the small *g*-tensor values are often due to a cancellation of the larger negative electronic and positive nuclear contributions. Furthermore, the electronic contribution clearly has an intimate relationship with the magnetizabilities and so the MREs and MAREs corresponding to this component should be more directly comparable. This is indeed the case, for example, the O-B97-3 method gives MRE and MARE values of 1.3% and 1.6%, respectively, which are very similar to the MRE and MARE values for the magnetizabilities of 1.4% and 1.4%, respectively.

Figure 4 presents a plot of the MRE relative to the benchmark set for the different methods. Again, the DFT functionals are grouped according to the information on which they are based. Except for the CAM-B3LYP, O-B3LYP, and O-CAM-B3LYP methods, all errors are larger in magnitude than the Hartree–Fock errors. The spread of the results within each functional grouping is also much larger. The KT2 functional, while still being the best GGA, offers a more modest improvement over the other GGAs. The best DFT method here is clearly the O-CAM-B3LYP method.

TABLE VIII. Magnetizabilities: Statistical errors for the DFT/aug-cc-pCVQZ results (excluding O_3) relative to the CCSD(T)/aug-cc-pCV[TQ]Z benchmark data set. All quantities are in SI units (10^{-30} J T^{-2}).

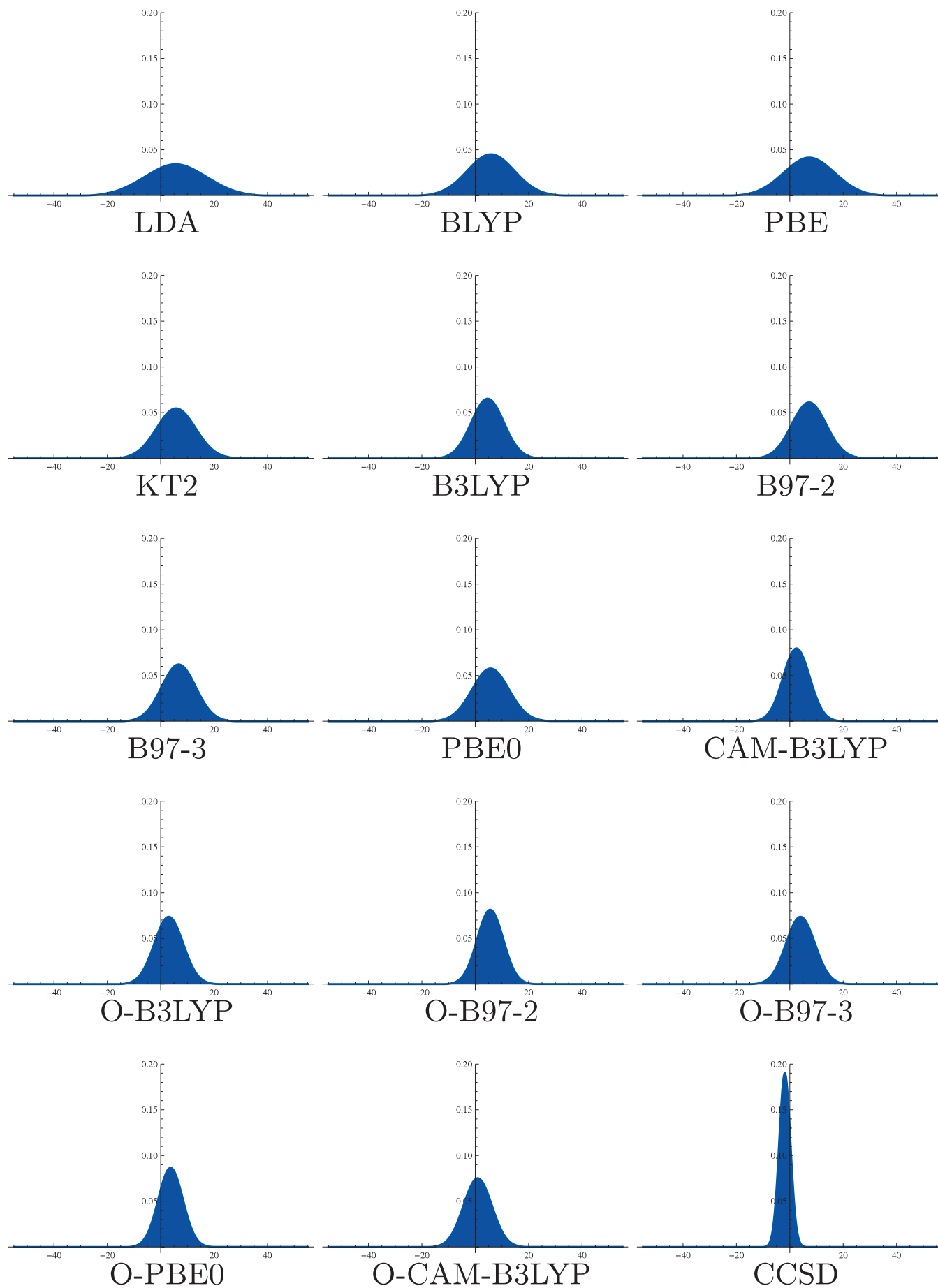|	LDA	BLYP	PBE	KT2	B3LYP	B97-2	B97-3	PBE0	CAM[a]
ME	5.4	5.7	7.1	5.6	4.5	7.1	6.6	5.6	2.4
MAE	9.6	8.0	9.2	6.5	5.5	7.2	6.6	6.0	3.8
MaxE	31.6	26.6	25.7	21.6	18.4	25.3	24.2	23.6	14.1
MRE	2.0	1.8	2.4	1.6	1.5	2.3	2.3	2.0	0.9
MARE	3.7	2.9	3.4	2.2	2.0	2.5	2.3	2.2	1.4
SD	11.5	8.8	9.5	7.3	6.1	6.5	6.4	6.9	5.0

[a]CAM-B3LYP functional.

FIG. 3. Normal distributions of the errors in magnetizabilities relative to the CCSD(T)/aug-cc-pCV[TQ]Z benchmark data set for the set of molecules excluding O_3 calculated using the aug-cc-pCVQZ basis set.

TABLE IX. Magnetizabilities: Statistics for the DFT-OEP/aug-cc-pCVQZ (excluding O_3) relative to the CCSD(T)/aug-cc-pCV[TQ]Z benchmark data set. All quantities are in SI units (10^{-30} J T^{-2}).

	O-B3LYP	O-B97-2	O-B97-3	O-PBE0	O-CAM[a]
ME	2.9	5.5	4.5	3.6	0.8
MAE	4.1	5.7	4.6	4.2	3.7
MaxE	17.4	17.9	16.8	15.5	15.1
MRE	0.8	1.6	1.4	1.1	0.2
MARE	1.4	1.8	1.4	1.4	1.2
SD	5.4	4.9	4.3	4.6	5.3

[a]O-CAM-B3LYP method.

C. Constrained search results

As has been done throughout the present work, the common approximation when calculating Kohn–Sham magnetic properties is to neglect the current dependence of the XC functional in a magnetic field, that is, $E_{xc}[\rho,\mathbf{j}] \approx E_{xc}[\rho]$. However, the size of this approximation is largely unknown and only a few implementations[89] for the calculation of molecular properties including current dependence explicitly have been made. Most of these use the Vignale–Rasolt–Geldart (VRG) XC functional.[90,91] While current-density effects are expected to be small, it is not clear in what cases the current is actually negligible. For example, Handy and co-workers[89] found that, for HF and H_2O, the effect of including current-dependent terms in the determination of magnetizabilities was of the order of 0.2×10^{-30} J T^{-2}. However, for CO and N_2, where a magnetic field perpendicular to the bond axis induces a strong paramagnetic current, the effect was more significant and of the order of $5-10 \times 10^{-30}$ J T^{-2}. In the context of Tables VIII and IX, such errors are not negligible. Similar errors are expected in the electronic part of the *g* tensor, although their impact is somewhat masked by cancellation with the nuclear contribution.

Since, in the present work, we computed CCSD and CCSD(T) results in a consistent fashion for comparison with Kohn–Sham DFT results, it is informative to consider Kohn–Sham calculations constrained to give the coupled-cluster densities.[12,13] To this end, we employ the constrained-search

procedure of Wu and Yang as outlined in Sec. II and Ref. 58. Specifically, we consider a subset of 15 molecules (HF, CO, $^{15}N_2$, H_2O, HC^{15}N, NH_3, CH_2O, CH_4, C_2H_4, CH_3F, FC^{15}N, H_2S, HCP, N_2O, and PN) and perform WY calculations in the aug-cc-pCVQZ basis set for the CCSD and CCSD(T) densities. The values obtained for the rotational *g* tensors and magnetizabilities may then be compared directly with their standard CCSD and CCSD(T) counterparts, see the results in the supplementary material.[27] If the current dependence of the XC functional was indeed negligible, then one would expect the WY results to be very similar to the CCSD and CCSD(T) ones.

From the error analysis of rotational *g* tensors in Table X, it is clear that the WY(CCSD) and WY[CCSD(T)] methods underestimate the CCSD and CCSD(T) results systematically. A similar systematic underestimation was observed when comparing DFT results to the benchmark data in Sec. IV A. Over this subset, our best DFT method O-B97-3 gives MRE, MARE, and SD values of -2.1%, 5.8%, and 0.0232, respectively, compared with the CCSD values; compared with the CCSD(T) values, the corresponding deviations are -0.5%, 4.7%, and 0.0153, respectively. Given that these errors are somewhat similar to those in Table X, it would seem desirable to investigate further the current dependence of the more accurate XC functionals in Table VI in an attempt to obtain higher accuracy. The inclusion of a current dependence may indeed aid in the interpretation of the results since, in the present case, for example, error cancellations may be introduced between the accuracy of the ground-state density obtained from a given XC functional and the lack of current dependence in the subsequent evaluation of the response properties.

For the magnetizabilities a similar trend is observed. The DFT functionals systematically overestimate the magnetizability in a similar fashion to the WY values, see Table XI.
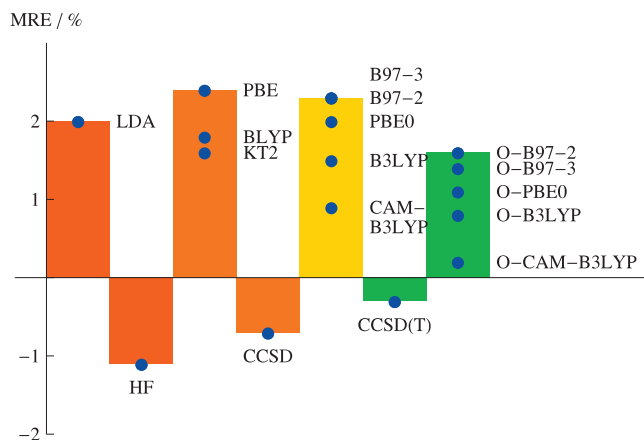

FIG. 4. MREs (%) in the calculation of magnetizabilities compared to the CCSD(T)/aug-cc-pCV[TQ]Z benchmark data set (excluding O_3) for the various wave function and DFT methods employed. The DFT results are grouped by functional type. The heights of the bars correspond to the largest MRE in each category.

TABLE X. Rotational *g* tensors: Statistical errors in WY(CC) values relative to the corresponding CC values (all-electron/aug-cc-pCVQZ values).

	WY(CCSD)	WY[CCSD(T)]
ME	−0.0094	−0.0122
MAE	0.0095	0.0122
MaxE	0.0821	0.0777
MRE	−2.7	−3.5
MARE	5.6	5.9
SD	0.0156	0.0183

TABLE XI. Magnetizabilities: Statistical errors in WY(CC) values relative to the corresponding CC values (all-electron/aug-cc-pCVQZ values). All quantities are in SI units (10^{-30} J T^{-2}).

	WY(CCSD)	WY[CCSD(T)]
ME	4.3	5.6
MAE	4.3	5.6
MaxE	13.4	19.9
MRE	1.5	2.0
MARE	1.5	2.0
SD	4.0	5.7

The best method is now the O-CAM-B3LYP method, giving MRE, MARE, and SD values of 0.3%, 1.4%, and 4.6, respectively, relative to the CCSD values and 0.0% 1.1%, and 3.6 relative to the CCSD(T) values. For HF and H_2O, the differences between the WY and coupled-cluster results we observe are small, consistent with the previous study of Handy and co-workers.[89] For N_2 and CO, however, the shifts are larger, consistent with the previous work, but have opposite sign. Given that the previous study did not adequately address the gauge-origin independence of the results obtained, further investigation of the current dependence is warranted.

V. CONCLUSIONS

In the present work, we calculated a set of benchmark rotational *g* tensors and magnetizabilities using (rotational) LAOs and coupled-cluster methods. The analysis of the basis-set dependence in Sec. IV A revealed the importance of augmenting the basis sets with diffuse functions rather than core-correlating functions and that reasonably converged results are obtained at the aug-cc-pCVQZ level. Extrapolation techniques were applied to the results from the two largest basis sets to give an estimate of the basis-set-limit quantities. We believe that this set of results provides a useful test set for benchmarking a variety of *ab initio* methods. This was corroborated in the case of rotational *g* tensors by a careful comparison with accurate experimental results.

In Sec. IV B, we used our benchmark data set to compare the accuracy of a variety of density functionals. The importance of considering vibrational corrections in comparison with experimental values for the rotational *g* tensors was clearly illustrated. Indeed, these corrections are essential to reveal the true accuracy of the coupled-cluster calculations. Conversely, they degrade the DFT results systematically, the results being close to experiment without the consideration of vibrational corrections but too low when these corrections are added. For the magnetizabilities, a comparison with experiment was not possible because of the large experimental error bars. However, a comparison with our benchmark set revealed that the variations between the quality of the different XC functionals are not large and the results are not comparable in quality to the coupled-cluster approaches. To reconcile this finding with the observations for the *g* tensors, the relationship between the two properties was discussed and relative errors for only the electronic contribution to the *g* tensors (the nuclear contribution being

method independent) were compared, revealing a similarity between the quality of the two properties at the various DFT levels. In this context, it is clear that the calculation of magnetizabilities and rotational *g* tensors remains difficult for DFT. It is noteworthy that, for both properties, the DFT and coupled-cluster values approach the benchmark values (or empirical equilibrium values) from opposite sides, the systematic nature of the improvements in the wave-function results being clearly evident in Figs. 2 and 4. While the DFT functionals grouped by category show a general trend of improvement, this trend is not systematic. For practical applications one must, as always, bear in mind that the systematic improvability and high accuracy of the coupled-cluster calculations comes at a much higher computational cost than is required for the DFT calculations.

The present study highlights the need for careful consideration of vibrational corrections when developing new approximations in DFT and evaluating existing ones, as illustrated by the fact that the KT2 results are close to experimental results but degrade when vibrational corrections are considered. This is not a surprising result since the data set on which this functional was trained did not fully and uniformly consider vibrational effects. The OEP evaluations clearly also benefit from some error cancellation when compared directly with experiment. However, the systematic improvement in moving from conventional to OEP evaluations of the same functionals still remain when compared with the benchmark values.

To make a more direct comparison between the DFT and coupled-cluster results, we considered DFT calculations constrained to give the coupled-cluster densities. In these calculations, as in the other DFT calculations presented in this paper, we employed the approximation $E_{xc}[\rho, \mathbf{j}] \approx E_{xc}[\rho]$, which is common practice in the calculation of DFT magnetic response properties. The results presented in Sec. IV C show that the errors in these WY calculations are similar to those observed for the "best" DFT functionals in the present study. Since one possible source of the difference between the WY values and the pure coupled-cluster numbers is the approximation introduced by neglecting the current dependence of the functional in the response calculation, we are led to suggest that further investigation of this dependence employing LAOs may be fruitful. Only a few implementations of current-dependent DFT have been presented and only a few current-dependent functionals have been proposed; the present benchmark set could provide useful data for benchmarking a current-dependent DFT implementation of magnetic response property calculations with LAOs.

[1] R. G. Parr and W. Yang, *Density-Functional Theory of Atoms and Molecules* (Oxford University Press, Oxford, 1989).

[2] W. Koch and M. C. Holthausen, *A Chemist's Guide to Density Functional Theory*, 2nd ed. (Wiley-VCH, Weinheim, 2001).

[3] T. Helgaker, P. Jørgensen, and J. Olsen, *Molecular Electronic-Structure Theory* (Wiley, New York, 2000).

[4] K. Ruud, T. Helgaker, K. L. Bak, P. Jørgensen, and H. J. A. Jensen, J. Chem. Phys. **99**, 3847 (1993).

[5] D. J. D. Wilson, C. E. Mohn, and T. Helgaker, J. Chem. Theory Comput. **1**, 877 (2005).

[6] J. Gauss, K. Ruud, and T. Helgaker, J. Chem. Phys. **105**, 2804 (1996).

[7] J. Gauss, K. Ruud, and M. Kállay, J. Chem. Phys. **127**, 074101 (2007).

[8] N. F. Ramsey, *Molecular Beams* (Clarendon, Oxford, 2000).

[9] W. H. Flygare and R. C. Benson, Mol. Phys. **20**, 225 (1971).

[10] W. H. Flygare, Chem. Rev. **74**, 653 (1974).

[11] O. B. Lutnæs, A. M. Teale, T. Helgaker, and D. J. Tozer, J. Chem. Theory Comput. **2**, 827 (2006).

[12] P. J. Wilson and D. J. Tozer, Chem. Phys. Lett. **337**, 341 (2001).

[13] M. J. Allen, T. W. Keal, and D. J. Tozer, Chem. Phys. Lett. **380**, 70 (2003).

[14] P. J. Wilson and D. J. Tozer, J. Mol. Struct. **602–603**, 191 (2002).

[15] A. J. Cohen, Q. Wu, and W. Yang, Chem. Phys. Lett. **399**, 84 (2004).

[16] A. M. Teale, A. J. Cohen, and D. J. Tozer, J. Chem. Phys. **126**, 074101 (2007).

[17] A. M. Teale and D. J. Tozer, Chem. Phys. Lett. **383**, 109 (2004).

[18] W. Hieringer, F. Della Sala, and A. Görling, Chem. Phys. Lett. **383**, 115 (2004).

[19] A. V. Arbuznikov and M. Kaupp, Chem. Phys. Lett. **386**, 8 (2004).

[20] A. V. Arbuznikov and M. Kaupp, Chem. Phys. Lett. **391**, 16 (2004).

[21] A. V. Arbuznikov and M. Kaupp, Int. J. Quantum Chem. **104**, 261 (2005).

[22] A. A. Auer, J. Gauss, and J. F. Stanton, J. Chem. Phys. **118**, 10407 (2003).

[23] M. E. Harding, M. Lenhart, A. A. Auer, and J. Gauss, J. Chem. Phys. **128**, 244111 (2008).

[24] R. T. Sharp and G. K. Horton, Phys. Rev. **90**, 317 (1953).

[25] J. D. Talman and W. F. Shadwick, Phys. Rev. A **14**, 36 (1976).

[26] M. Levy, Proc. Natl. Acad. Sci. U.S.A. **76**, 6062 (1979).

[27] See EPAPS supplementary material http://dx.doi.org/10.1063/1.3242081 for data and error analysis in other basis sets.

[28] A. E. Hansen and T. D. Bouman, J. Chem. Phys. **82**, 5035 (1985).

[29] F. London, J. Phys. Radium **8**, 397 (1937).

[30] R. M. Stevens, R. M. Pitzer, and W. N. Lipscomb, J. Chem. Phys. **38**, 550 (1963).

[31] H. M. Kelly and P. W. Fowler, Chem. Phys. Lett. **206**, 568 (1993).

[32] K. Ruud and T. Helgaker, Chem. Phys. Lett. **264**, 17 (1997).

[33] J. F. Ogilvie, S. L. Cheah, Y. P. Lee, and S. P. A. Sauer, Theor. Chim. Acta **108**, 85 (2002).

[34] P.-O. Åstrand, K. Ruud, K. V. Mikkelsen, and T. Helgaker, Mol. Phys. **92**, 89 (1997).

[35] P.-O. Åstrand, K. Ruud, K. V. Mikkelsen, and T. Helgaker, J. Chem. Phys. **110**, 9463 (1999).

[36] K. Ruud, T. Helgaker, and P. Jørgensen, J. Chem. Phys. **107**, 10599 (1997).

[37] K. Ruud, J. Vaara, J. Lounila, and T. Helgaker, Chem. Phys. Lett. **297**, 467 (1998).

[38] C. E. Mohn, O. B. Lutnæs, D. J. D. Wilson, T. Helgaker, and K. Ruud, Adv. Quantum Chem. **50**, 77 (2005).

[39] S. P. A. Sauer, Adv. Quantum Chem. **48**, 319 (2005).

[40] K. Ruud, P.-O. Åstrand, and P. R. Taylor, J. Chem. Phys. **112**, 2668 (2000).

[41] S. M. Cybulski and D. M. Bishop, J. Chem. Phys. **106**, 4082 (1997).

[42] S. M. Cybulski and D. M. Bishop, J. Chem. Phys. **100**, 2019 (1994).

[43] J. Oddershede and J. R. Sabin, Chem. Phys. **122**, 291 (1988).

[44] S. P. A. Sauer, V. Špirko, I. Paidarová, and J. Oddershede, Chem. Phys. **184**, 1 (1994).

[45] S. P. A. Sauer, V. Špirko, and J. Oddershede, Chem. Phys. **153**, 189 (1991).

[46] S. P. A. Sauer and J. F. Ogilvie, J. Phys. Chem. **98**, 8617 (1994).

[47] J. F. Ogilvie, J. Oddershede, and S. P. A. Sauer, Chem. Phys. Lett. **228**, 183 (1994).

[48] J. Geertsen and G. E. Scuseria, J. Chem. Phys. **90**, 6486 (1989).

[49] S. P. A. Sauer, J. Oddershede, and J. Geertsen, Mol. Phys. **76**, 445 (1992).

[50] S. P. A. Sauer, Chem. Phys. Lett. **260**, 271 (1996).

[51] K. Ruud, P.-O. Åstrand, T. Helgaker, and K. V. Mikkelsen, J. Mol. Struct.: THEOCHEM **388**, 231 (1996).

[52] P.-O. Åstrand, K. Ruud, K. V. Mikkelsen, and T. Helgaker, Chem. Phys. Lett. **271**, 163 (1997).

[53] K. L. Bak, S. P. A. Sauer, J. Oddershede, and J. F. Ogilvie, Phys. Chem. Chem. Phys. **271**, 163 (2005).

[54] P. J. Wilson, R. D. Amos, and N. C. Handy, J. Mol. Struct. **506**, 335 (2005).

[55] W. Yang and Q. Wu, Phys. Rev. Lett. **89**, 143002 (2002).

[56] Q. Wu and W. Yang, J. Theor. Comput. Chem. **2**, 627 (2003).

[57] E. Fermi and E. Amaldi, Mem. Accad. Italia. **6**, 117 (1934); reproduced in E. Fermi "Collected Papers: (Note e Memorie)", loc. cit., as art No. 82.

[58] Q. Wu and W. Yang, J. Chem. Phys. **118**, 2498 (2003).

[59] T. H. Dunning, Jr., J. Chem. Phys. **90**, 1007 (1989).

[60] R. A. Kendall, T. H. Dunning, Jr., and R. J. Harrison, J. Chem. Phys. **96**, 6796 (1992).

[61] D. E. Woon and T. H. Dunning, Jr., J. Chem. Phys. **100**, 2975 (1994).

[62] D. E. Woon and T. H. Dunning, Jr., J. Chem. Phys. **103**, 4572 (1995).

[63] G. D. Purvis III and R. J. Bartlett, J. Chem. Phys. **76**, 1910 (1982).

[64] K. Raghavachari, G. W. Trucks, J. A. Pople, and M. Head-Gordon, Chem. Phys. Lett. **157**, 479 (1989).

[65] A. Halkier, T. Helgaker, P. Jørgensen, W. Klopper, and J. Olsen, Chem. Phys. Lett. **302**, 437 (1999).

[66] A. Halkier, T. Helgaker, P. Jørgensen, W. Klopper, H. Koch, J. Olsen, and A. K. Wilson, Chem. Phys. Lett. **286**, 243 (1998).

[67] P. Hohenberg and W. Kohn, Phys. Rev. B **136**, B864 (1964).

[68] S. J. Vosko, L. Wilk, and M. Nusair, Can. J. Phys. **58**, 1200 (1980).

[69] A. D. Becke, Phys. Rev. A **38**, 3098 (1988).

[70] C. Lee, W. Yang, and R. G. Parr, Phys. Rev. B **37**, 785 (1988).

[71] J. P. Perdew, K. Burke, and M. Ernzerhof, Phys. Rev. Lett. **77**, 3865 (1996).

[72] T. W. Keal and D. J. Tozer, J. Chem. Phys. **119**, 3015 (2003).

[73] P. J. Stephens, F. J. Devlin, C. F. Chabalowski, and M. J. Frisch, J. Phys. Chem. **98**, 11623 (1994).

[74] A. D. Becke, J. Chem. Phys. **98**, 5648 (1993).

[75] P. J. Wilson, T. J. Bradley, and D. J. Tozer, J. Chem. Phys. **115**, 9233 (2001).

[76] T. W. Keal and D. J. Tozer, J. Chem. Phys. **123**, 121103 (2005).

[77] C. Adamo and V. Barone, J. Chem. Phys. **110**, 6158 (1999).

[78] T. Yanai, D. P. Tew, and N. C. Handy, Chem. Phys. Lett. **393**, 51 (2004).

[79] ACESII, Mainz-Austin-Budapest Version 2007. See http://www.aces2.de.

[80] DALTON, Release 2.0, 2005. See http://www.kjemi.uio.no/software/dalton/dalton.html.

[81] I. Grabowski, S. Hirata, S. Ivanov, and R. J. Bartlett, J. Chem. Phys. **116**, 4415 (2002).

[82] I. V. Schweigert, V. F. Lotrich, and R. J. Bartlett, J. Chem. Phys. **125**, 104108 (2006).

[83] I. Grabowski, V. Lotrich, and R. J. Bartlett, J. Chem. Phys. **127**, 154111 (2007).

[84] F. Furche, Phys. Rev. B **64**, 195120 (2001).

[85] F. Furche and T. V. Voorhis, J. Chem. Phys. **122**, 164106 (2005).

[86] F. Furche, J. Chem. Phys. **129**, 114105 (2008).

[87] G. E. Scuseria, T. M. Henderson, and D. C. Sorensen, J. Chem. Phys. **129**, 231101 (2008).

[88] B. G. Janesko, T. M. Henderson and G. E. Scuseria, J. Chem. Phys. **130**, 081105 (2009).

[89] A. M. Lee, S. M. Colwell, and N. C. Handy, Chem. Phys. Lett. **229**, 225 (1994).

[90] G. Vignale, M. Rasolt, and D. J. W. Geldart, Phys. Rev. B **37**, 2502 (1988).

[91] G. Vignale, M. Rasolt, and D. J. W. Geldart, Adv. Quantum Chem. **21**, 235 (1990).

[92] S. M. Bass, R. L. DeLeon, and J. S. Muenter, J. Chem. Phys. **86**, 4305 (1987).

[93] I. Ozier, P. N. Yi, A. Khosla, and N. F. Ramsey, J. Chem. Phys. **46**, 1530 (1967).

[94] S. I. Chan, M. R. Baker, and N. F. Ramsey, Phys. Rev. **136**, A1224 (1964).

[95] W. H. Flygare, R. L. Shoemaker, and W. Hüttner, J. Chem. Phys. **50**, 2414 (1969).

[96] J. Verhoeven and A. Dymanus, J. Chem. Phys. **52**, 3222 (1970).

[97] S. L. Hartford, W. C. Allen, C. L. Norris, E. F. Pearson, and W. H. Flygare, Chem. Phys. Lett. **18**, 153 (1973).

[98] S. L. Rock, E. F. Pearson, E. H. Appleman, C. H. Norris, and W. H. Flygare, J. Chem. Phys. **59**, 3940 (1973).

[99] W. L. Meerts, S. Stolte, and A. Dymanus, Chem. Phys. **19**, 467 (1977).

[100] W. Hüttner, U. E. Frank, W. Majer, K. Mayer, and V. Špirko, Mol. Phys. **64**, 1233 (1988).

[101] C. H. Anderson and N. F. Ramsey, Phys. Rev. **149**, 14 (1966).

[102] R. Honerjaeger and R. Tischer, Z. Naturforsch. A **29**, 342 (1974).

[103] C. L. Norris, E. F. Pearson, and W. H. Flygare, J. Chem. Phys. **60**, 1758 (1974).

[104] R. C. Benson and W. H. Flygare, J. Chem. Phys. **51**, 3087 (1969).

[105] R. L. Shoemaker and W. H. Flygare, Chem. Phys. Lett. **2**, 610 (1968).

[106] S. L. Rock, J. C. McGurk, and W. H. Flygare, Chem. Phys. Lett. **19**, 153 (1973).

[107] C. A. Burrus, J. Chem. Phys. **30**, 976 (1959).

[108] S. L. Rock, J. K. Hancock, and W. H. Flygare, J. Chem. Phys. **54**, 3450 (1971).

[109] W. Hüttner, P. D. Foster, and W. H. Flygare, J. Chem. Phys. **50**, 1710 (1969).

[110] F. Mehran, R. A. Brooks, and N. F. Ramsey, Phys. Rev. **141**, 93 (1966).

[111] R. R. Freeman, A. R. Jacobson, D. W. Johnson, and N. F. Ramsey, J. Chem. Phys. **63**, 2597 (1975).

[112] J. M. L. J. Reinartz, W. L. Meerts, and A. Dymanus, Chem. Phys. **31**, 19 (1978).

[113] F. H. de Leeuw and A. Dymanus, Chem. Phys. Lett. **7**, 288 (1970).

[114] J. M. Pochan, R. G. Stone, and W. H. Flygare, J. Chem. Phys. **51**, 4278 (1969).

[115] D. H. Sutter, W. Hüttner, and W. H. Flygare, J. Chem. Phys. **50**, 2869 (1969).

[116] A. W. Ellenbroek and A. Dymanus, Chem. Phys. Lett. **42**, 303 (1976).